Quasar microlensing and THESEUS

Mimoza Hafizi, Lindita Hamolli,
University of Tirana,
Albania

III International Workshop on recent LHC Physics results and related topics
10-12 October 2018, Tirana, Albania

Content

Basics of Gravitational Lensing

Microlensing

Quasar Microlensing

THESEUS (The Transient High-Energy Sky and Early Universe Surveyor) and Quasar Microlensing

I. Basics of Gravitational Lensing

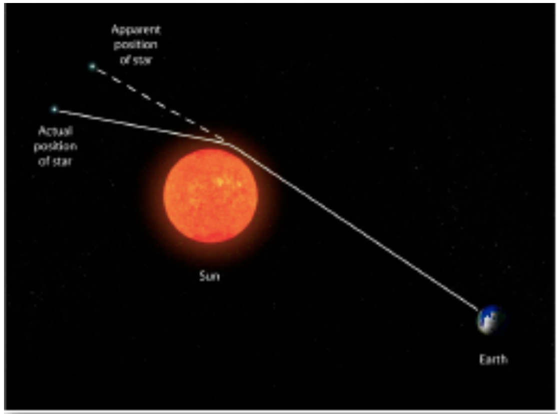

A light ray passing close to a mass distribution, is bent. Its path is changed (slightly).

General Relativity (Einstein, 1916) **predicted** $\alpha = 4GM / bc^2$, **2x larger than Newtonian. 1919 Eclipse.**

Straight alignment and compact spherical lens distribution → Einstein Ring.

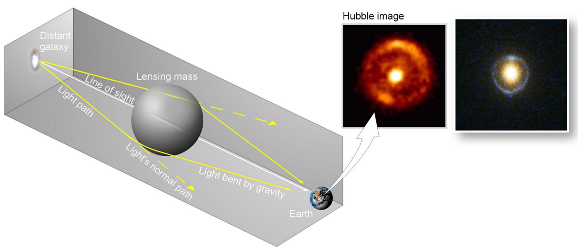

B1938+666 discovered in radio; arcsec-diameter Einstein ring; image taken by **HST** in IR; lensing galaxy z=0.878.

SDSS J162746.44-005357.5; 0.1 arcmin-diameter Einstein ring; **HST+SDSS** in optical and IR; lensing galaxy z=0.207.

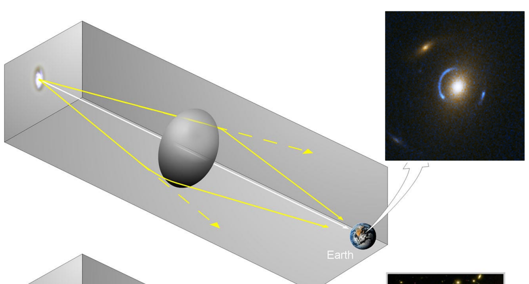

Misalignment → Arc segments.

SDSS J120540.43+491029.3; 0.1 arcmin-diameter arcs; **HST+SDSS** in optical and IR; lensing galaxy z=0.214.

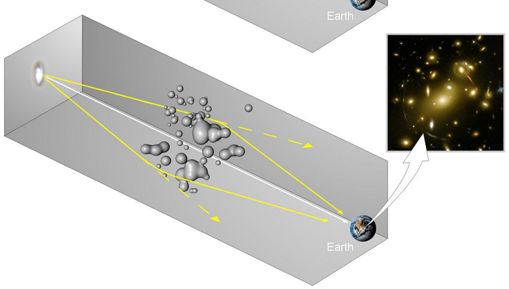

Complex distribution of lensing mass (galaxy groups and clusters) → Multiple and distorted images of the same source.

Abell 2218, z=0.1756, **HST.**

I. Basics of Gravitational Lensing

Theory

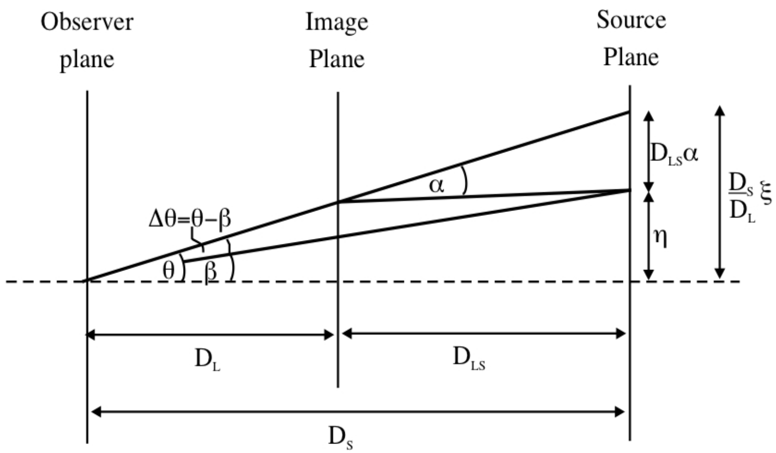

$\theta - \beta = \alpha D_{LS} / D_S$, **lens eqn.**

$\alpha = 4GM / bc^2$, **deflection eqn.**

Images-where both eqns. satisfied

Effective lensing potential, projection of the three-dimensional Newtonian potential on the lens plane (and rescaled). Its gradient, deflection angle.

$$\Psi(\vec{\theta}) = \frac{D_{LS}}{D_L D_S} \frac{2}{c^2} \int \Phi(D_L \vec{\theta}, z) dz$$

Jacobian matrix A, transformation of coordinates from source **Y** to lens **X**

$$A = \frac{\partial \vec{y}}{\partial \vec{x}} = \left(\delta_{ij} - \frac{\partial^2 \Psi(\vec{x})}{\partial x_i \partial x_j} \right)$$

Det A

I. Basics of Gravitational Lensing

Image Properties

Photons are neither created nor destroyed by the GL, the surface brightness of the source-unchanged, but can be magnified/demagnified and/or distorted.

- **Magnification**-the inverse of **Det A** (first order considerations). It is ideally infinite in those points where Det A=0, which lie on ***critical lines*** on the lens plane. Close to them, the images are strongly distorted. The source points, generating images around critical lines are located along ***caustics***.

- **Distortion**
  a) Two eigenvalues of matrix A (first order considerations): **convergence** (isotropic distortion) and **shear** (stretching along a privileged direction)
  b) **Flexions**, second order considerations. Introduce other anisotropies.

- **Time delays** between images of the same source. Two origins, geometric (length of the path) and gravitational (slowing down of photons)

- **Polarization is not changed**

- **GL is independent on wavelength**

I. Basics of Gravitational Lensing

Three Classes

A) Strong lensing (few hundred cases discovered up to now). High distortions, Einstein rings, arcs and multiple images. Produced by galaxies or galaxy clusters which lie close to the line of sight of the source and develop critical lines (det A=0).

- Gravitational telescopes;
- Estimate the dark matter-in large scales;
- Estimate the mass distribution at the Universe;
- Measure distances and Hubble constant (by counting the number of lenses, the time delay); $H_0 = 71.9^{+2.4}_{-3}$ km/s/Mpc (***Bonvin et al. 2017***).

Galaxy Cluster SDSS J1004+4112 (HST).

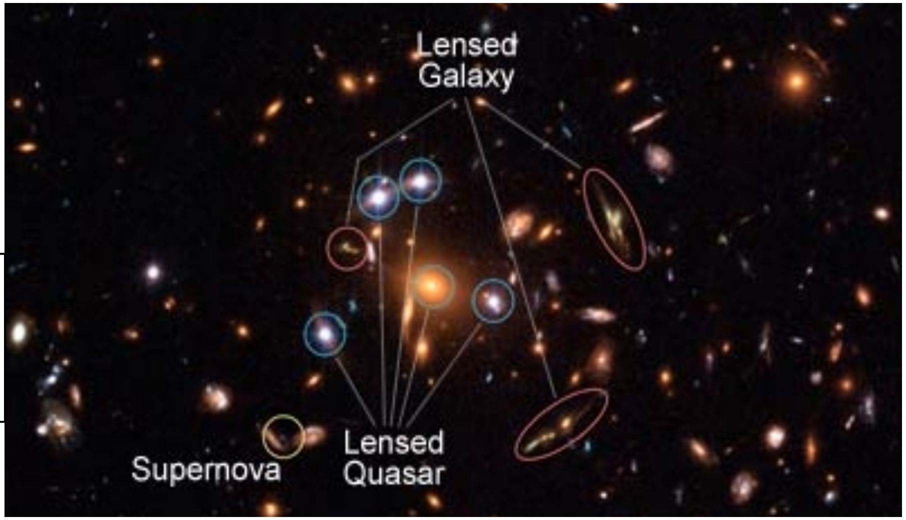

I. Basics of Gravitational Lensing

Three Classes

B) Weak lensing. Much smaller distortions. Produced by galaxies or galaxy clusters, whose angular separation to the line of sight is relatively large.

A statistical estimation of the lensing effect (high number of galaxies in the field of view): dark matter and mass distribution.

"Topographical map" of the dark matter in the Bullet Cluster, detected using weak lensing (Miyazaki et al., 2015)

C) Microlensing. No visible distortions, but a variable magnification of observed light. Lensing objects are stars, exoplanets and other small astrophysical bodies.

- Discover exoplanets
- Count the dark matter in Galaxy (a mean stellar/dark matter contribution to 7%/93%), ***Krawcsynski et al. 2018***

II. Microlensing

Gravitational microlensing is the action of compact objects (inside their Einstein ring) of small mass ($10^{-6}<M/M_S<10^3$) along the line of sight to compact distant sources (quasars, stars)

Einstein, 1936, Paczynski, 1986

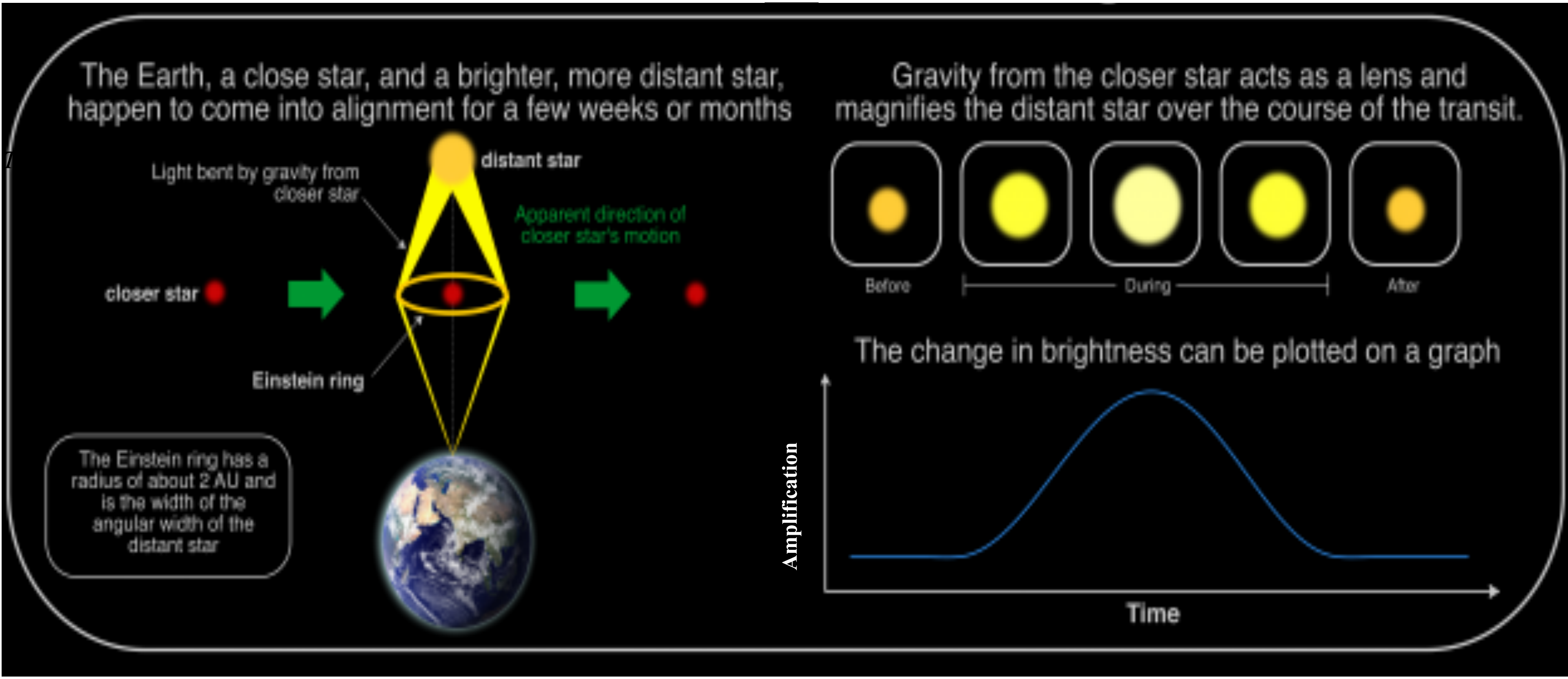

II. Microlensing

Observables and Parameters

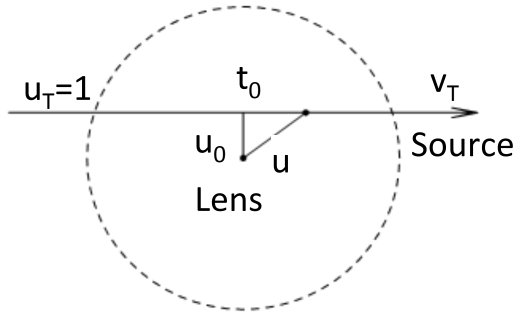

Projection of the source trajectory in the lens plane

Dashed line is the Einstein Ring;

When trajectory is on the Einstein Ring, A=1.34;

The maximum of A depends on the impact parameter u_0

From the standard light curve, one can find T_E and u_0

If we know the lens velocity and distance, its mass can be defined;

If not, values of mass, velocity and distance are degenerated inside a sole relation.

Einstein radius, ≈ A.U. or fractions, inside Galaxy

$$R_E = \sqrt{\frac{4GM}{c^2}\frac{D_{LS}D_L}{D_S}}$$

Einstein Time, ≈ months (hours or days for planets), inside Galaxy

$$T_E = \frac{R_E}{v_T}$$

Einstein Angle, ≈ milliarsec

$$\Theta_E = \sqrt{\frac{4GM}{c^2}\frac{D_{LS}}{D_L D_S}}$$

Amplification *A*

$$A(u) = \frac{u^2(t)+2}{u(t)\sqrt{u^2(t)+4}}$$

with

$$u(t) = \sqrt{u_0^2 + (\frac{t-t_0}{T_E})^2}$$

II. Microlensing

Second order effects

Help to add relations between mass, velocity and distance and remove degeneracy of their values.

Finite source effects

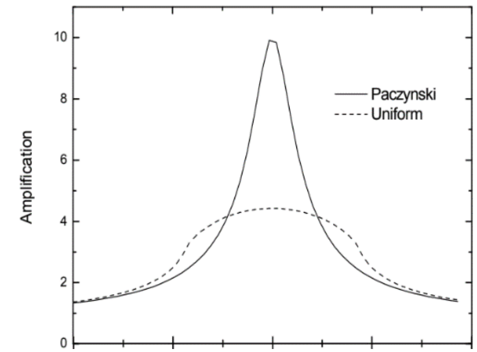

Hamolli et al., 2015, Adv. Astron. ID 402303

Parallax effects

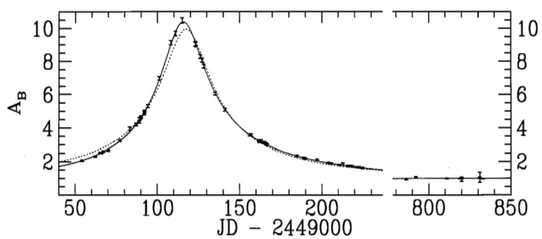

Alcock et al., 1995, ApJ, 454, 125

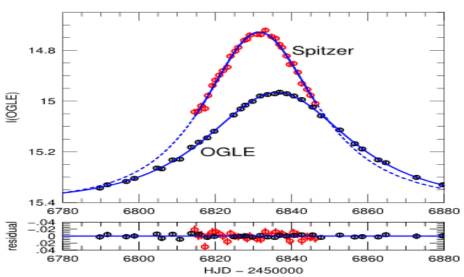

Yee et al., 2015, ApJ, 802, 76

- **Orbital parallax**, observer revolution
- **Trigonometric parallax**, observation by two telescopes

Astrometric Observations

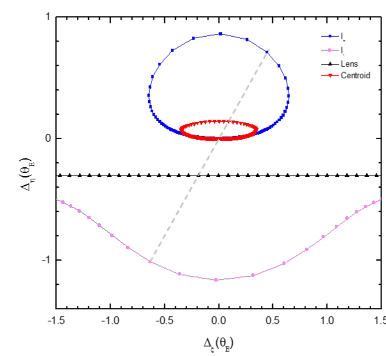

Hamolli et al., 2018, Ap&SS. 363, 153

Measurement of the position of **centroid**

II. Microlensing
Binary lens, exoplanets

First exoplanet: **OGLE-2003-BLG-235Lb**
Last exoplanet: **OGLE-2017-BLG-1522L b**

3823 confirmed exoplanets

- ~ 74 %, Transit method
- ~ 20 %, Radial Velocity method
- ~ 2 %, Gravitational Microlensing

Websites:
exoplanetarchive.ipac.caltech.edu
exoplanet.eu

Advantages:
Distances from Earth, up to the Galaxy center (tens of thousands light-years)
Moderate to large **distances from their own star**

A complementary method

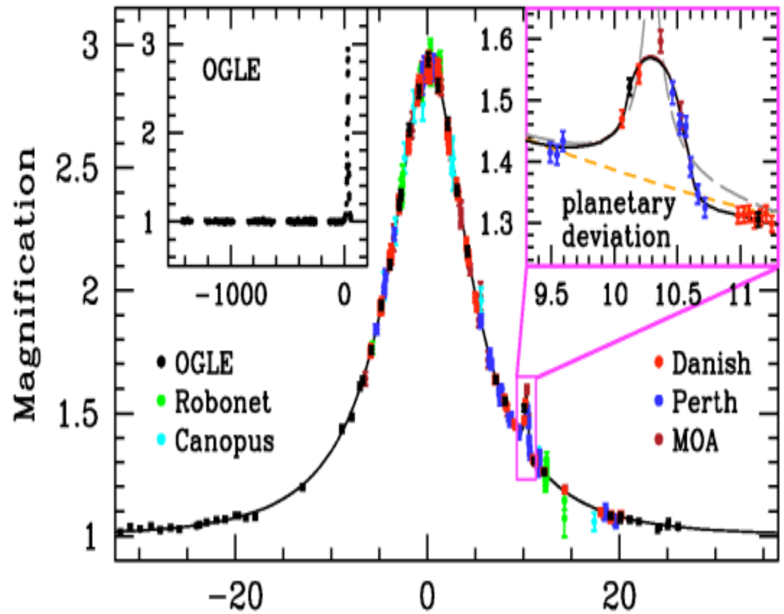

Light curve of OGLE-2005-BLG-390
21,500 light-years from Earth,
Planet's mass, 5.5 Earth mass
Semi-major axis, 2.6 AU
Beaulieu et al. 2006

II. Microlensing
Free floating Planets (FFP)

- Population of objects with M <0.01M_S, not orbiting around any host star.

- Uncertain origin

- Formed in protoplanetary disks and subsequently ejected?

Veras et al., 2012

- Formed via direct collapse of molecular clouds?

Silk, J. 1997

Gravitational Microlensing is a unique way to observe FFP

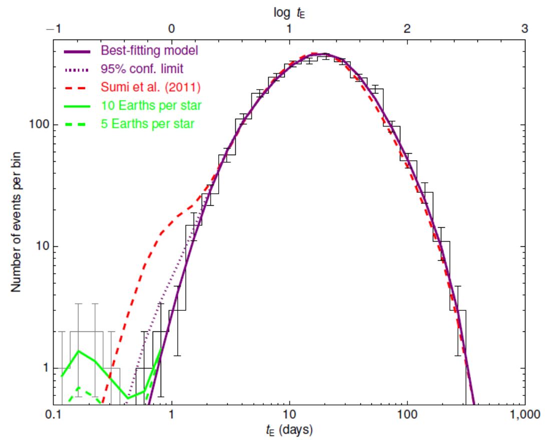

- From 474 microlensing events of MOA-II data set (2006-2007), 10 were found with T_E <2 days (red line), ***Sumi, et al., 2011.***
- A best fit procedure defines a mass range of FFPs $10^{-5} \leq M/M_S \leq 10^{-2}$, distributed following a power-law mass function $M^{-\alpha}$, with $\alpha = 1.3^{+0.3}_{-0.4}$ and number $N = 5.5^{+18.1}_{-4.3}$ of planetary mass objects per star (large uncertainty of low mass lens estimate).
- Recently there are some reviewed values for the mass distribution, by the analysis of 2617 events of OGLE-IV, 2010-2015: one Jupiter mass FFP for four stars ***Mroz, et al. 2017.***

II. Microlensing
Observations

- First missions, EROS (1990), MACHO (1992), OGLE (1992) and MOA (1995). Observations towards LMC, SMC and BULGE.
- The first two microlensing events are detected by MACHO towards LMC. Duration ~30 days, mass ~10^{-2}-$1M_S$, *Alcock, et al., 1993*
- In Tirana University, we study microlensing events caused by FFPs.
- We (Tirana University) estimate the optical depth (~10^{-8}); we predict the number of events (for future Euclid, WFIRST);

Optical depth, probability that at any time a random source is magnified more than the threshold amplification:

$$\tau = \int_0^{D_S} n(D_L)\pi R_E^2 dD_L$$

- We calculate statistically the probabilities to observe second order effects in the case of FFP: orbital parallax effect ~ 30%; finite source effect ~ 30%, *Hamolli et al. 2015;* trigonometric parallax (~ 74% OGLE-K2C9, ~ 25% for OGLE-Spitzer), *Hamolli et al. 2017.*
- We estimate the efficiency of astrometric signal on photometrically detected microlensing events (~ 6.5%, Gaia telescope), *Hamolli et al. 2018.*

II. Microlensing

Current and future missions

Present

- **OGLE**, since 1992, OGLE IV since 2009. Discovered more than 40 exoplanets towards the bulge. The first exoplanet is **OGLE-2003-BLG-235Lb**, $M=2.6M_J$, Semi-Major Axis=4.3AU. The last is **OGLE-2017-BLG-1522L b**, $M=0.75M_J$, Semi-Major Axis=0.59AU.

- **MOA**, since 1995. Discovered 21 exoplanets. The first exoplanet is **MOA-2007-BLG-192L b**, $M=0.0104M_J$, Semi-Major Axis=0.62.AU. The last is **MOA-2016-BLG-227L b**, $M=2.8M_J$, Semi-Major Axis=1.67AU

- **Gaia**, Astrometric Observations
- **Spitzer,** trigonometric parallax with OGLE and MOA

Future

- **WFIRST**, in 2020

- **Euclid**, in 2021

III. Quasar Microlensing

- QM is the lensing effect on quasar light, caused by compact objects in the **mass range** $10^{-6} \leq M/M_S \leq 10^3$, inside a lens galaxy.
- **Critical value** for the **surface mass density** Σ of the lensing galaxy:

$$\Sigma_{crit} = \frac{c^2}{4\pi G}\frac{D_S}{D_L D_{LS}}$$

Under Σ_{crit}, low probability for lensing and microlensing.

- The convergence of the lensing system has the value Σ/Σ_{crit} and equals the optical depth (source compactness).
- Recent studies show that quasar micro-lensing provides a possibility to probe extragalactic planets in the lens galaxy (***Dai et al., 2018***).
- What about THESEUS?

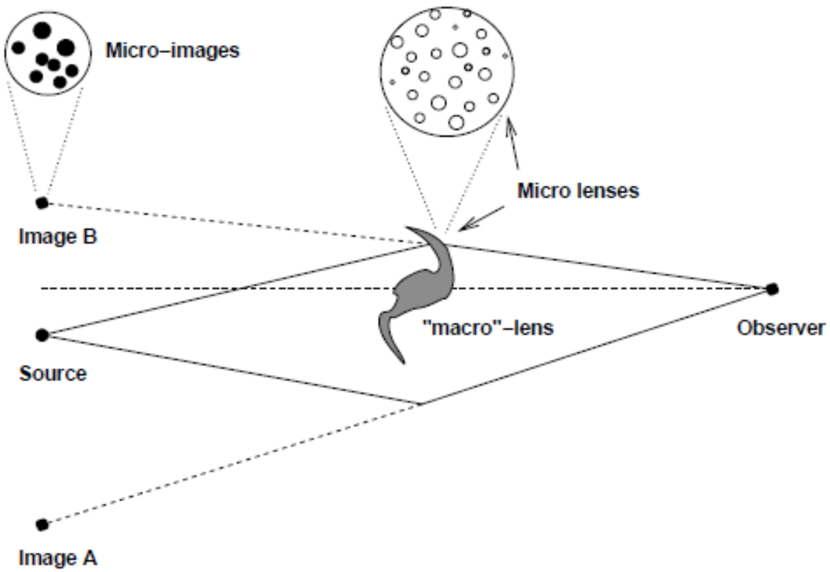

A schematic presentation of Quasar Microlensing

III. Quasar Microlensing

Parameters

- Quasars are **compact sources** relative to **small mass** galactic objects.

The size of their **continuum emitting region** $\approx 10^{13} m$

Einstein radius of stars at these distances $\approx 10^{14} m$

(z_L=0.5, z_Q=2)

Einstein radius of Earth-like planets at these distances

$\approx 10^{11} m$

- Einstein Angle $\approx \mu arc\sec$, unobservable
- But micro-image configurations change in time
- Lensing time scale (V_Q=600km/s), **several years**, too large
- Crossing caustic lines time scale, **some months**

- Based on variability of the image.
- Possible to be observed in case of a multiple-lensed quasar.
  - **The change in two images, effect of microlensing**
- Mean image separation in images is 1-2 arcsec.

$$R_{E,stars} = \sqrt{\frac{4GM}{c^2}\frac{D_{LQ}D_L}{DQ}}$$

$$\approx 4x10^{14}\left(\frac{M}{M_{Sun}}\right)^{1/2} m$$

$$\approx 7x10^{11}\left(\frac{M}{M_{Earth}}\right)^{1/2} m$$

$$\Theta_E = \sqrt{\frac{4GM}{c^2}\frac{D_{LQ}}{D_Q D_L}}$$

$$\approx 1.8\left(\frac{M}{M_{Sun}}\right)^{1/2} \mu arc\sec$$

$$t_E = R_E / V_Q \approx 15\left(\frac{M}{M_{Sun}}\right) years$$

$$t_{cross} = R_Q / V_Q \approx months$$

III. Quasar Microlensing

Caustics

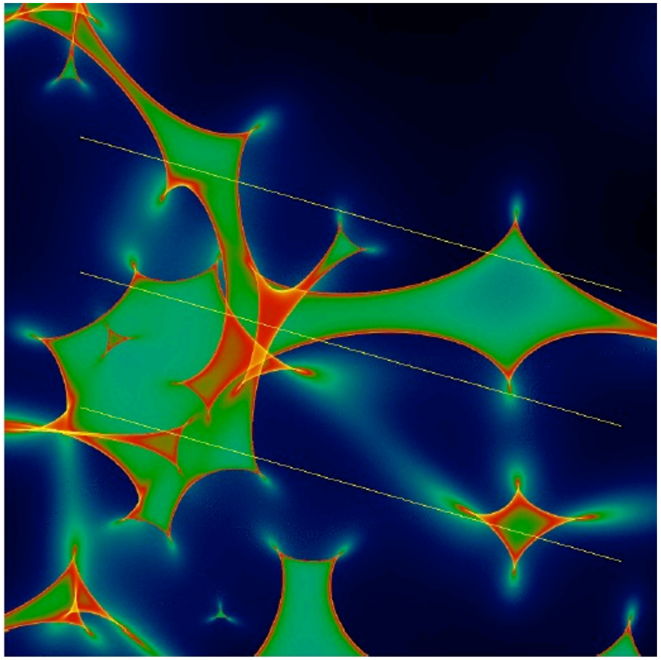

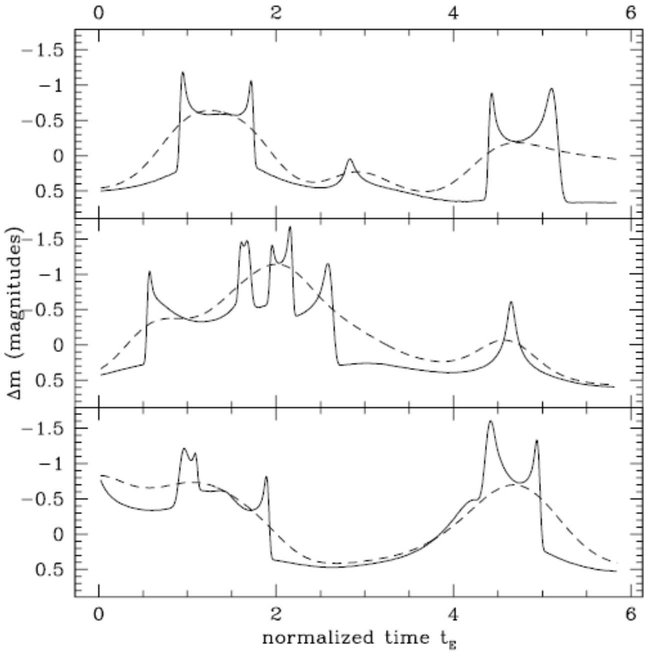

- Left. **Microlensing magnification pattern**, produced by stars in a lensing galaxy. The colors represent different magnifications (-0.5,-1.5,0.5), with the sharp caustic lines, corresponding to the highest magnification. Three *dashed lines* indicate three tracks, along which a background quasar moves.
- Right. The corresponding light curves, ***Wambsganss, J. (1998)***

III. Quasar Microlensing

Comparision

	Galactic microlensing	Quasar microlensing
Lenses	Stars, planets, Machos in Galaxy (SMC, LMC, M31)	Stars and planets in a far lensing galaxy
Sources	Stars at Galaxy and Local Group	Quasars
Einstein Angle	milliarcsec	microarcsec
Einstein time	Days-weeks-months	Months-years
Optical depth	10^{-6}	about 1
Proposed by	Einstein 1936, Paczynski 1986	Chang&Refsdal 1979
First detected	OGLE, MACHO, EROS 1993	Irwing et al. 1989 mission
Good for	Machos, stars, planets	Dark matter, cosmological parameters, quasar profiles

III. Quasar Microlensing

Stellar mass lenses

Name	Type	Distance	Observatory	Reference
QSO 2237+0305	Quadruple (5th-X) lensed	z_Q=1.7 z_L=0.04	VLT (optic) Chandra (X)	***Wambsganss et al., 1990, ApJ, 352, 407***
Q0957+561	Double lensed	z_Q=1.4 z_L=0.36	Rosat (X) Apache PO (optic)	***Wambsganss et al., 2000, A&A, 362, 37***
PG 1115+080	Quadruple lensed	z_Q=1.722 z_L=0.3?	Maidanak (optic) Chandra (X)	***Pooley et al., 2006, ApJ, 648, 67***
SDSS J0924+0219	Quadruple lensed	z_Q=1.524 z_L=0.394	SDSS (optic) Chandra (X)	***MacLeod et al., 2015, ApJ, 806, 258***
HE 0435−1223	Quadruple lensed	z_Q=1.689 z_L=0.46	SDSS (optic) Chandra (X)	***Blackburne et al., 2014, ApJ, 789, 125***

III. Quasar Microlensing

Planetary mass Objects-RXJ 1131-1231

- RXJ1131-1231, quadruple lensed, $z_s = 0.658$ and $z_L = 0.295$, giant elliptical galaxy.
- Smaller emission region, extragalactic planets
- Spectroscopic analysis. FeKα line-different emission regions with different energy shifts $g=E_o/E$, due to the special (Doppler) and general relativistic (gravitational).
- Hot bright corona of the accretion disk. The photon energies encode information about where originated.
- The line energy shift occurs when a microlensing caustic lands on the source region, such that a portion of the disk with different g is magnified differently.
- High frequency of shifts-microlensing effect.
- Planet mass fraction to 2,000 objects (from Moon to Jupiter sizes) per main sequence star.

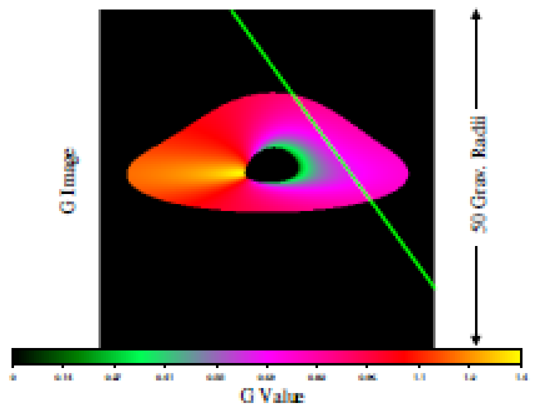

$M_{BH}=1.3x10^8 M_S$, $R_g=1.9x10^{11}$m, $R_{EP}=7.9x10^{13}$m

Theoretical map of energy shifts.

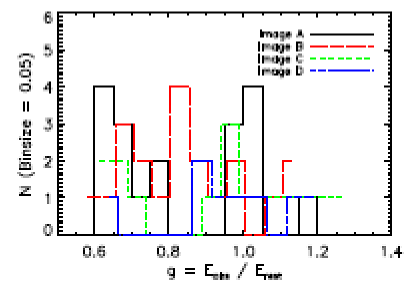

Distributions of the FeKα line energy shifts, measured in the four quasar images.

Dai et al., 2018

IV. THESEUS
Mission

- **THESEUS** is a mission concept, proposed in response to the ESA call for medium-size mission (M5), within the Cosmic Vision Program
- Is selected by ESA, on May 7, 2018, to enter an assessment phase study (two rival missions, Envision, Spica)
- To be in space in 2032
- Mission designation:

Explore the Early Universe (cosmic dawn and reionization era) by unveiling a complete census of the Gamma-Ray Burst (GRB) population in the first billion years.

- Several countries present. Albania

* Planck (2009-2013), microwave length. CMB

- Euclid (2021), near infrared.

Dark energy, dark matter, Universe Acceleration

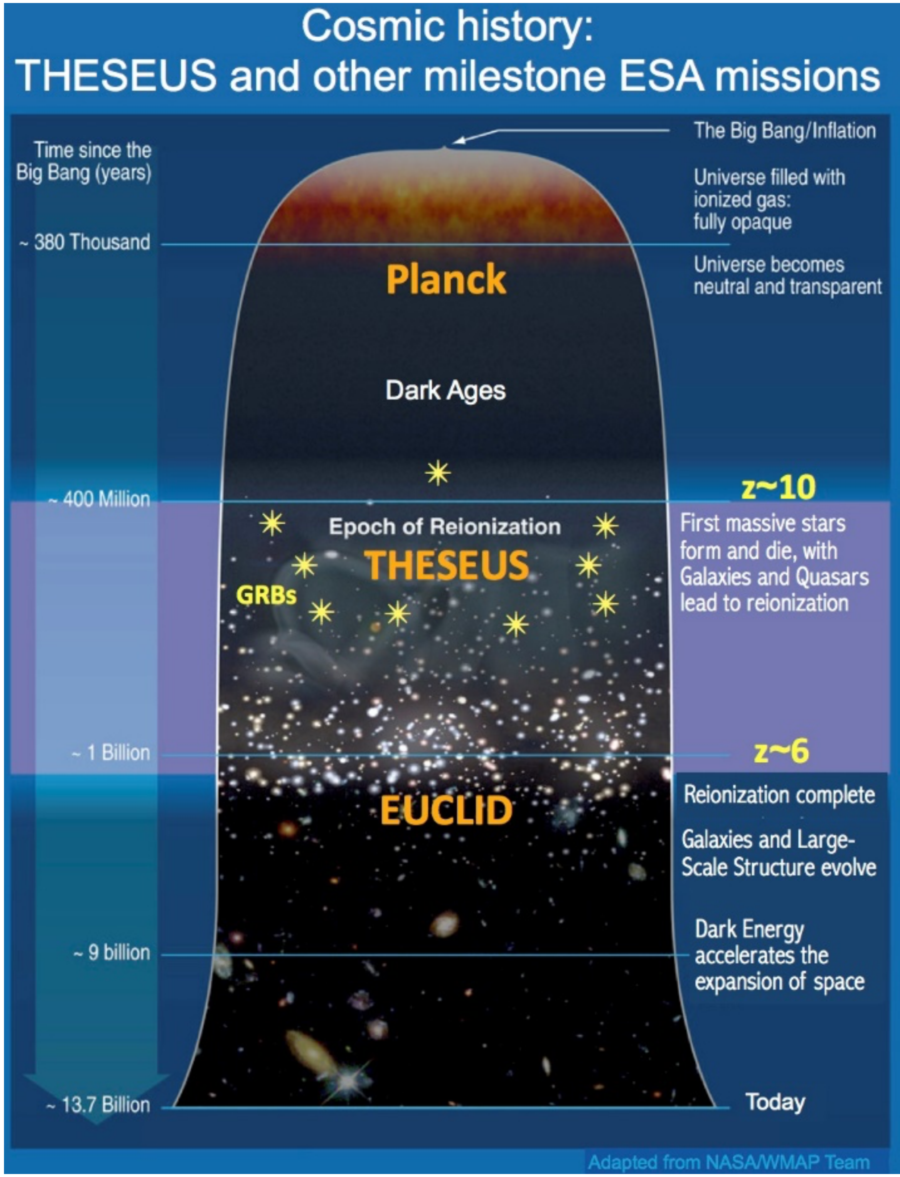

IV. THESEUS
Payload

A **unique payload,** providing a combination of:

- Wide and deep sky monitoring in a broad energy band (0.3keV - 20 MeV)-XGIS+SXI;
- Focusing capabilities in the soft X-ray band-SXI;

Soft X-ray Imager (SXI, 0.3 – 6 keV): a set of 4 lobster-eye telescopes units;

X-Gamma rays Imaging Spectrometer (XGIS, 2 keV – 20 MeV), a set of three detectors.

- On board **near-IR 70cm telescope**, for immediate transient identification and redshift determination-IRT.

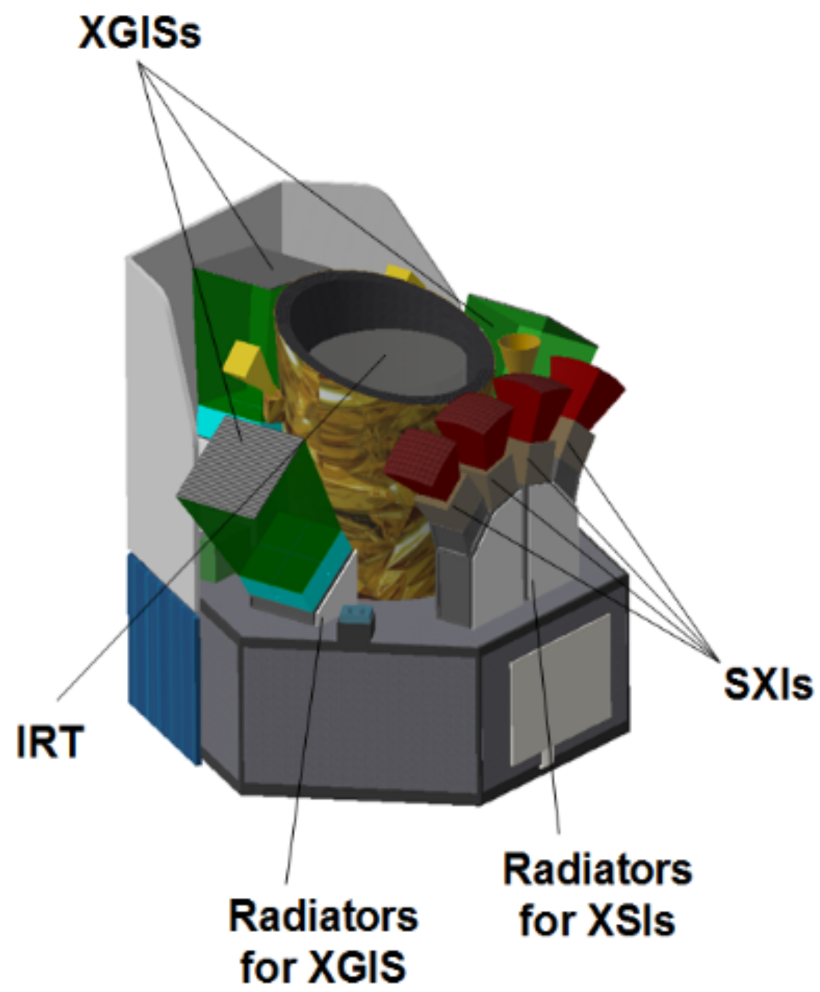

https://www.isdc.unige.ch/theseus/

IV. THESEUS

Sensitivity

THESEUS will exploit an all-sky X-ray monitoring of high sensitivity, carried out at high cadence:

Soft X-ray Imager (SXI, 0.3 – 6 keV): a total field of view (FOV) of ~1sr with source location accuracy < 1';

X-Gamma rays Imaging Spectrometer (XGIS, 2 keV – 20 MeV): a ~1.5sr FOV, a source location accuracy of ~5' arcmin;

SXI provides the capability to monitor the X-ray flux of hundreds of AGN with about 10% accuracy on daily timescales, and hundreds more on longer timescales.
AGN, 350/year

The THESEUS space mission concept: science case, design and expected performances-
arXiv:1710.04638v4 [astro-ph.IM] 27 Mar 2018

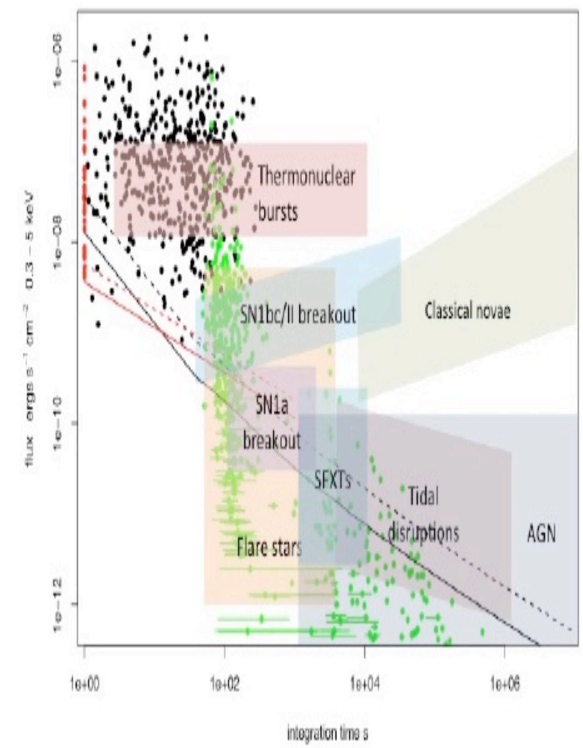

Figure 4: Sensitivity of the SXI (black curves) and XGIS (red) vs. integration time. The solid curves assume a source column density of 5×10^{20} cm^{-2} (i.e., well out of the Galactic plane and very little intrinsic absorption). The dotted curves assume a source column density of 10^{22} cm^{-2} (significant intrinsic absorption). The black dots are the peak fluxes for Swift BAT GRBs plotted against T90/2. The flux in the soft band 0.3-10 keV was estimated using the T90 BAT spectral fit including the absorption from the XRT spectral fit. The red dots are those GRBs for which T90/2 is less than 1 s. The green dots are the initial fluxes and times since trigger at the start of the Swift XRT GRB light-curves. The horizontal lines indicate the duration of the first time bin in the XRT light-curve. The various shaded regions illustrate variability and flux regions for different types of transients and variable sources.

IV. THESEUS

THESEUS versus Chandra

	Range (KeV)	FOV	Accuracy	Sensitivity erg/cm^2/s (in 104s)
Theseus SXI/ Chandra ACIS	**(0.3 – 6) /(0.4-10)**	1srd/17x17 arcmin (10^4-10^5 higher)	**10-20 arcsec /1 arcsec**	**10^{-9} / 4×10^{-15}**
Theseus XGIS/ Chandra HRC	**(2KeV –20MeV)/ (0.4-10)KeV**	1.5srd/30x30 arcmin (10^4-10^5 higher)	**5 arcsmin/0.4 arcsec**	**10^{-10}/10^{-16}**

THESEUS-a unique combination of huge FOV, angular resolution and sensitivity

**ACIS- Advanced CCD Imaging Spectrometer; HRC-High Resolution Camera*

IV. THESEUS and Quasar Microlensing

Some Conclusions

- The survey strategy of THESEUS will permit an observation of the longterm variability of an unprecedentedly large AGN sample, at depths never reached before.
- New Quasars will be observed, with smaller Enstein Radius of lensing bodies, shorter Einstein times → smaller quasar regions to be probed and closer to the central Black Hole, shorter variability.
- Higher sensitivity to study X ray lines (FeKα), precious sources of information for the different regions of the accretion disk.
- We need to look for **new methods** for discerning microlensing traces from other variability inside quasar images.

Bibliography

- Einstein, A. 1916, AnP, 354,769
- Bonvin et al., 2017, MNRAS, 465, 4914B
- Miyazaki et al., 2015, ApJ, 807, 22
- Krawcsynski et al., arxiv: 1809.01057
- Einstein A., 1936, Science, 84, 506
- Paczynski B., 1986, 304, 1.
- Beaulieu et al., Nature, 439, 437
- Veras, D. & Raymond, S. N. 2012, MNRAS, 421, 117
- Silk, J. 1997, ASIC, 502, 111
- Sumi et al. 2011, Nature, 473, 349
- Mroz et al., 2017, 548, 183
- Alcock et al., 1993, Nature, 365, 621
- Hamolli et al., 2015, Adv. Astron. ID 402303
- Hamolli et al., 2017, AstBu. 72, 73
- Hamolli et al., 2018, Ap&SS. 363, 153
- Dai et al., 2018 , ApJ, 853, 27
- Wambsganss, J.   1998, LRR, 1, 2
- Pooley et al. 2007, ApJ, 661, 19